Magnetic Resonance in Medicine 45:756–764 (2001)

# Detection of Myocardial Viability Based on Measurement of Sodium Content: A $^{23}$Na-NMR Study

Michael Horn,[1*] Claudia Weidensteiner,[2] Heike Scheffer,[1] Martin Meininger,[1] Mark de Groot,[1] Helga Remkes,[1] Charlotte Dienesch,[1] Karin Przyklenk,[3] Markus von Kienlin,[2] and Stefan Neubauer[1]

**MRI of total sodium (Na) content may allow assessment of myocardial viability, but information on Na content in normal myocardium, necrotic/scar tissue, and stunned or hibernating myocardium is lacking. Thus, the aims of the study were to: 1) quantify the temporal changes in myocardial Na content post-myocardial infarction (MI) in a rat model (Protocol 1); 2) compare Na in normally perfused, hibernating, and stunned canine myocardium (Protocol 2); and 3) determine whether, in buffer-perfused rat hearts, infarct scar can be differentiated from intact myocardium by $^{23}$Na-MRI (Protocol 3). In Protocol 1, rats were subjected to LAD ligation. Infarct/scar tissue was excised at control and 1, 3, 7, 28, 56, and 128 days post-MI ($N$ = 6–8 each), Na content was determined by $^{23}$Na-NMR spectroscopy (MRS) and ion chromatography. Na content was persistently increased at all time points post-MI averaging 306*–160*% of control values (*$P$ < 0.0083 vs. control). In Protocol 2, $^{23}$Na-MRS of control (baseline), stunned and hibernating samples revealed no difference in Na. In Protocol 3, $^{23}$Na-MRI revealed a mean increase in signal intensity, to 142 ± 6% of control values, in scar tissue. A threshold of 2 standard deviations of the image intensity allowed determination of infarct size, correlating with histologically determined infarct size ($r$ = 0.91, $P$ < 0.0001). Magn Reson Med 45:756–764, 2001. © 2001 Wiley-Liss, Inc.**

**Key words: $^{23}$Na NMR; viability; myocardial infarction; hibernating; stunning; 3D-CSI**

In patients with a large akinetic myocardial region, assessment of myocardial viability is frequently required to decide on further therapy. Specifically, while scarred tissue cannot recover function and does not need revascularization, viable but hibernating myocardium will usually resume contractile function after revascularization with percutaneous transluminal coronary angiography (PTCA) or bypass surgery, whereas viable but stunned myocardium will recover spontaneously over time. Although it is well recognized that preoperative viability assessment is predictive of postoperative prognosis (1), all current methods to assess myocardial viability have intrinsic problems, such as patient discomfort and procedural risk (stress testing with inotropic agents using echocardiography (2) or MRI (3)), dependence on acoustic window (echocardiography), low specificity ($^{201}$T1-scintigraphy) or limited availability (PET) (4).

Experimental $^{23}$Na-MRI was first reported by DeLayre et al. (5) in the isolated heart, and applied in vivo by Ra et al. (6) in humans. $^{23}$Na is among the nuclei offering the potential for the highest spatial MRI resolution due to its high NMR sensitivity and short $T_1$, thereby allowing for short pulse repetition times. Considerable evidence indicates that ionic homeostasis is perturbed and tissue Na content is substantially increased during the initial hours, days after myocardial infarction (7–9). However, long-term changes in tissue Na content during postinfarction healing and scar formation have not been reported.

We propose that if Na content is persistently and selectively increased in nonviable (i.e., necrotic or scarred) regions of the heart, $^{23}$Na-MRI could provide the basis for distinguishing necrotic/scarred vs. viable myocardium and delineating infarct size. Thus, the purpose of our study was threefold: 1) to quantify temporal changes in myocardial Na content at 1–128 days after myocardial infarction in the rat model of coronary artery ligation (Protocol 1); 2) to determine, in dog hearts, if dysfunctional but viable myocardium (stunned or hibernating) shows alteration in $^{23}$Na content when compared with baseline control values (Protocol 2); and 3) to assess, at 1 month postinfarction in rat hearts, whether scarred vs. normal myocardium can be distinguished (and infarct size can be quantified) by means of experimental $^{23}$Na-MRI (Protocol 3).

## METHODS

### Experimental Myocardial Infarction: Rat Model (Protocols 1 and 3)

Myocardial infarction (MI) was induced in Wistar rats by permanent ligation of the left anterior descending (LAD) coronary artery, as described previously (10,11). Total surgical mortality was approximately 40%. For surviving rats, group assignments were made at 1 day post-MI. Control animals were not operated prior to use. All rats received commercial rat chow and water ad libitum. All procedures conformed with the guiding principles of the American Physiological Society.

### Experimental Protocols: Rat Model (Protocols 1 and 3)

In Protocol 1, seven groups of rats were studied with $^{23}$Na MRS: control (no infarct), and 1, 3, 7, 28, 56, and 128 days after MI ($N$ = 6, 8, 8, 6, 7, 8, and 6, respectively). At the time of sacrifice, rats were anesthetized with 30–50 mg pentobarbital i.p. Hearts were excised and bathed in cold (4°C) $LiCl/CaCl_2$ solution to prevent non iso-osmolar con-

[1]Medizinische Universitätsklinik, [2]Physikalisches Institut, Würzburg University, Würzburg, Germany.

[3]Heart Institute, Good Samaritan Hospital, Los Angeles, California.

Grant sponsor: IZKF Würzburg University (from BMBF); Grant number: 01 KS 9603 (Projekt F1); Grant sponsor: SFB 355 Würzburg University; Grant number: TP A3.

*Correspondence to: Michael Horn, Ph.D., Medizinische Universitätsklinik, Josef-Schneider-Str. 2, 97080 Würzburg, Germany.
E-mail: m.horn@mail.uni-wuerzburg.de

Received 27 March 2000; revised 20 November 2000; accepted 28 November 2000.

ditions and cell leakage due to membrane damage. The necrotic/scar region was identified by gross morphologic appearance: while noninfarcted myocardium is reddish, the infarcted left ventricular (LV) wall (observed 3 days post-MI) appears flaccid and red-brown, and the evolving scar (in groups sampled ≥ 1 week after coronary artery ligation) is thin, stiff, and yellow-white in color. For each heart, the infarct/scar was excised and washed in LiCl/$CaCl_2$ solution to remove residual blood. Each infarct/scar was separated into two specimens for determination of: 1) $^{23}$Na MRS (total $^{23}$Na content); and 2) dry weight/wet weight ratio (edema formation) and ion chromatography (total $^{23}$Na content as reference). The infarct/scar samples had a mean weight of 27.8 ± 1.4 mg (range 6.8–61.8 mg, size approximately 12–72 mm$^3$).

For $^{23}$Na-MRI (Protocol 3), rats were killed 4 weeks after MI. The hearts were excised and perfused isovolumically (balloon in LV) with Krebs-Henseleit buffer at constant pressure (100 mm Hg), as previously described (12). Heart rate, LV-developed pressure, and coronary flow were continuously monitored. To ensure stable physiological conditions, total experimental time was limited to 1 hr.

### Hibernating and Stunned Myocardium: Dog Model (Protocol 2)

In three pentobarbital-anesthetized open-chest mongrel dogs, coronary flow was reduced to 57 ± 1% of baseline for 3 hr by application of a stenosis around the LAD, as previously described (13). Transmural needle biopsies were taken from the center of the LAD territory at baseline ($N$ = 5), 3 hrs after application of the stenosis (short-term hibernation; $N$ = 3) and 30 min postreperfusion (flow restored to 136 ± 16% of baseline: stunned; $N$ = 4). Samples were immediately frozen in liquid nitrogen and kept at −80°C. At the time of analysis, biopsies were allowed to thaw, immediately weighed (mean 30.8 ± 2.2 mg) and used for $^{23}$Na NMR measurement, as described below. The canine experiments were approved by the Institutional Animal Care and Use Committee of Good Samaritan Hospital, and conformed with the guiding principles of the American Physiological Society.

### Standards and Solutions

For $^{23}$Na-MRS, a solution of 119.7 mg NaCl in 60% $D_2O$/40% $H_2O$ with 10 mM dysprosium shift reagent (as $Tris_3$[Dy(TTHA)]) (14) was used as an external standard. The tissue specimen was placed in the inner tube (5 mm OD) of a set of two coaxial tubes, while the outer tube was filled with the external standard solution. The tissue was bathed in an iso-osmolar mixture of 149.6 mM LiCl and physiological [$Ca^{2+}$] of 1.25 mM. All chemicals were purchased from Sigma-Aldrich Chemie (Deisenhofen, Germany) and used without further purification.

### $^{23}$Na-MRS (Protocols 1 and 2)

$^{23}$Na-NMR spectra were obtained on a Bruker AM 300 using a 10-mm multinuclear probe. Before acquiring spectra, the homogeneity of the $B_0$ field was optimized by shimming on the $^2$D-lock level. We used a 10-mm NMR tube (Wilmad, Buena, NJ) filled with $^{23}$Na standard solution and equipped with a Wilmad special stem coaxial insert of 5 mm for the infarct/scar tissue. As described above, the sample was placed in the inner coaxial NMR tube and bathed in LiCl/$CaCl_2$ solution. The tissue was placed in the center of the sensitive volume of the RF coil and was kept in position by adhesion. An Aspect 3000 computer (Bruker, Rheinstetten, Germany) was used in the pulsed Fourier transform mode to generate $^{23}$Na-NMR spectra at 79.50 MHz. Single spectra were accumulated over 8.62-min periods, averaging data from 1000 free induction decays (FIDs) obtained using a pulse time of 20 μs, a pulse angle of approximately 80°, and an interpulse delay of 0.52 sec. Sweep width was 20000 Hz, and dead time between excitation and data acquisition was 62.5 μs. FIDs were multiplied with a Gauss filter (center of Gauss multiplication at 25% of FID, 7 Hz line width modulation), Fourier transformed and individually phase-corrected. Both the interpulse delay of 62.5 μs and the Gauss multiplication favor extracellular Na signal with narrow resonances. Fast relaxing components of the $^{23}$Na signal, which show broad signals due to short $T_2$ values, are suppressed by this method. In the resulting $^{23}$Na spectra, shifts in the $^{23}$Na signal from the standard solution and scar tissue resulted in two completely resolved resonances. Resonance areas were measured using the Bruker DISNMR89 integration routine. Due to short $T_1$ values (28.8 msec at 8.5 T (15); $T_1$ = 34.2 msec (7) in myocardium and $T_1$ = 26.2 msec (7) in the infarct at 4.7 T) of $^{23}$Na, all spectra are fully relaxed. In each $^{23}$Na-NMR spectrum, the area of the standard resonance was set to 100 and the signal arising from tissue was expressed relative to the standard peak area. Absolute concentrations were determined by comparison to three phantoms of defined sodium content. In a subgroup of samples, we performed $^{23}$Na MRS of the LiCl/$CaCl_2$ solution after removal of the biopsy. No $^{23}$Na signal was detected, thereby confirming that leakage of $^{23}$Na from the tissue was negligible.

### Ion Chromatography (Protocol 1)

Dried tissue samples were placed in a platinum-iridium crucible (ÖGUSSA, Vienna, Austria). After adding nitric acid (1–2 ml: TraceSelect grade, Fluka, Deisenhofen, Germany), the sample was heated to 300°C and cooled to room temperature. This sequence was repeated a total of three times. During the final acid treatment the solution was reduced to high viscosity. The residue was dissolved in 2 ml of water, filtered (35 μm), and 1.5 ml of the filtrate was diluted for measurement of sodium content by ion chromatography. We used an IonPac C12 column (stationary phase) and 1% hydrochloric acid (mobile phase) with a Dionex chromatography system (Dionex Corp., Sunnyvale, CA) and conductivity detection.

### Dry Weight/Wet Weight Ratio (Protocol 1)

Tissue samples were weighed at the time of collection, and after being dried at 55°C for 3 days. The dry weight/wet weight ratio was then calculated.

### $^{23}$Na-MRI (Protocol 3)

In isolated hearts assessed 4 weeks post-MI, experiments were performed on a Bruker AMX-500 microscopy system

using a custom-built $^{23}$Na probehead (two-ring birdcage resonator with an inner diameter of 24 mm) tuned to the $^{23}$Na frequency of 132.15 MHz. Shimming was performed on the sodium signal, resulting in a line width of approximately 14 Hz.

The 3D $^{23}$Na gradient-echo dataset was acquired in approximately 13 min with a repetition time of 30 msec (32 averages, no gating). Pulse angle was optimized to yield maximum signal for the given acquisition parameters. The thickness of the excited slice was limited to 25 mm (covering the whole heart) in the z-direction. The spatial resolution was 0.75 mm in the x- and y-directions (horizontal plane) and 2 mm in the z-direction, yielding a voxel size of 1.125 μl. The matrix size of the dataset was $32 \times 32 \times 16$; after zero filling, it was $256 \times 256 \times 16$.

The sweep width was kept low at 1280 Hz to ensure a low-noise bandwidth, which improves the signal-to-noise ratio (SNR) (16). Blurring was avoided since the sweep width was larger than the product of the line width of the sodium signal and the time domain ($TD = 32$). Echo time was 7 msec.

$^{1}$H fast low-angle shot (FLASH) imaging was done after $^{23}$Na MRI to define cardiac anatomy. The $^{23}$Na probehead was exchanged with a custom-built $^{1}$H probehead (two-ring birdcage resonator with an inner diameter of 24 mm) without changing the position of the heart in the magnet. A multislice dataset with a spatial resolution of 0.094 mm $\times$ 0.188 mm $\times$ 1 mm was acquired. Contrast between the perfusate and the tissue was enhanced with an off-resonant MTC-pulse prior to excitation (17,18). The sequence was synchronized to the heart cycle.

### Infarct Size Measurement (Protocol 3)

#### *Histology*

After $^{23}$Na-MRI, all hearts were fixed in formalin, embedded in paraffin, and cut in cross-section at a thickness of 20 μm, at intervals of 1 mm. For histologic determination of infarct size, the slices were stained with Picrosirius Red (with this method, scar tissue appears red, while viable tissue stains yellow).

The stained sections were mounted on slides and digitally scanned. Using the software "NIH Image" (Wayne Rasband, National Institute of Health, Bethesda, MD) and computerized planimetry, we quantified the outer circumference of the heart, the circumference of the left ventricular chamber, and scar lengths measured along both the endo- and epicardial surfaces. Only areas where the scar occupied 50% or more of the LV wall were considered for planimetry. For each slice, the relative infarct size was calculated as (mean of the endo- and epicardial scar length)/(mean total wall length), as previously described (19). Results obtained from two adjacent histologic sections (spanning a thickness of 2 mm) were averaged, in order to match the 2-mm spatial resolution (z-direction) of the $^{23}$Na-NMR images.

#### *$^{23}$Na-MRI*

In two to four adjacent slices of the $^{23}$Na-MRI data set, the mean signal intensity of normal myocardium (i.e., remote from the scarred area or from ventricular cavities) and its standard deviation was measured. The $^{23}$Na-NMR images were corrected for $B_1$ inhomogeneity. Regions in the anterior wall of the heart were defined as scarred when the signal intensity exceeded a threshold of two times the standard deviation of the mean signal intensity of normal myocardium. LV and scar dimensions were measured using NIH image and planimetry, with analysis limited to areas where the scar occupied $> 50\%$ of the LV wall. Relative infarct size for slices in the 3D NMR data set was calculated using the same formula as that applied to the histologic sections. Regression analysis was employed to correlate infarct sizes measured from the $^{23}$Na-NMR image data set with the results from the corresponding histologic slices.

Mean signal intensity and SNR were determined in three adjacent slices of the $^{23}$Na-MRI data set (without $B_1$ correction) in a region in normal myocardium, in the scar, and in perfusate by averaging the intensity of 400 to 1000 pixels in the Fourier-transformed and zero-filled data. The contrast-to-noise ratio (CNR) between normal myocardium and the scar was calculated. SNR was defined as the (mean of the signal intensity)/(standard deviation of noise). CNR was defined as the (difference in signal intensity)/(standard deviation of noise).

### Data Analysis

In Protocol 1, each parameter quantified in the six post-MI groups was compared with its matched control (noninfarcted) value using the unpaired, two-tailed *t*-test. A Bonferroni correction for six comparisons was applied, and *P*-values $< 0.0083$ were considered significant. Total Na content in each sample measured by $^{23}$Na-MRS vs. ion chromatography was compared using a two-tailed, paired *t*-test, with *P*-values $< 0.05$ considered significant. Calculations were performed using StatView 4.51 software (Abacus Concepts Inc., Berkeley, CA). All data are reported as mean ± SEM, unless stated otherwise.

For Protocol 2, each parameter quantified in the two treated groups was compared with its matched control value using the unpaired, two-tailed *t*-test. A Bonferroni correction for two comparisons was applied, and *P*-values $< 0.025$ were considered significant (StatView 4.51).

Processing of the MRI data sets (Protocol 3) was performed with custom-written software in the IDL computing environment (Interactive Data Language, Research Systems Inc., Boulder, CO). Using matched data obtained from 19 slices, relative infarct sizes measured by $^{23}$Na-MRI vs. histology were compared by regression analysis (StatView 4.51).

## RESULTS

### Protocol 1

#### *Dry Weight/Wet Weight Ratios*

There was, as expected, significant edema in infarcted myocardium sampled at 1 and 3 days after coronary artery ligation: dry weight/wet weight ratios averaged 0.25 ± 0.0 in control hearts vs. 0.23 ± 0.01* and 0.18 ± 0.03* on days 1 and 3 post-MI. At later time points, scar tissue had a dry weight/wet weight ratio of 0.27 ± 0.03, 0.22 ± 0.07, 0.24 ± 0.02, and 0.18 ± 0.01 (days 7, 28, 56, and 128, respectively; $P$ = ns vs. control).

#### *$^{23}$Na-NMR Spectroscopy*

A typical $^{23}$Na-NMR spectrum of a myocardial sample shows a single resonance at 0 ppm and the resonance of

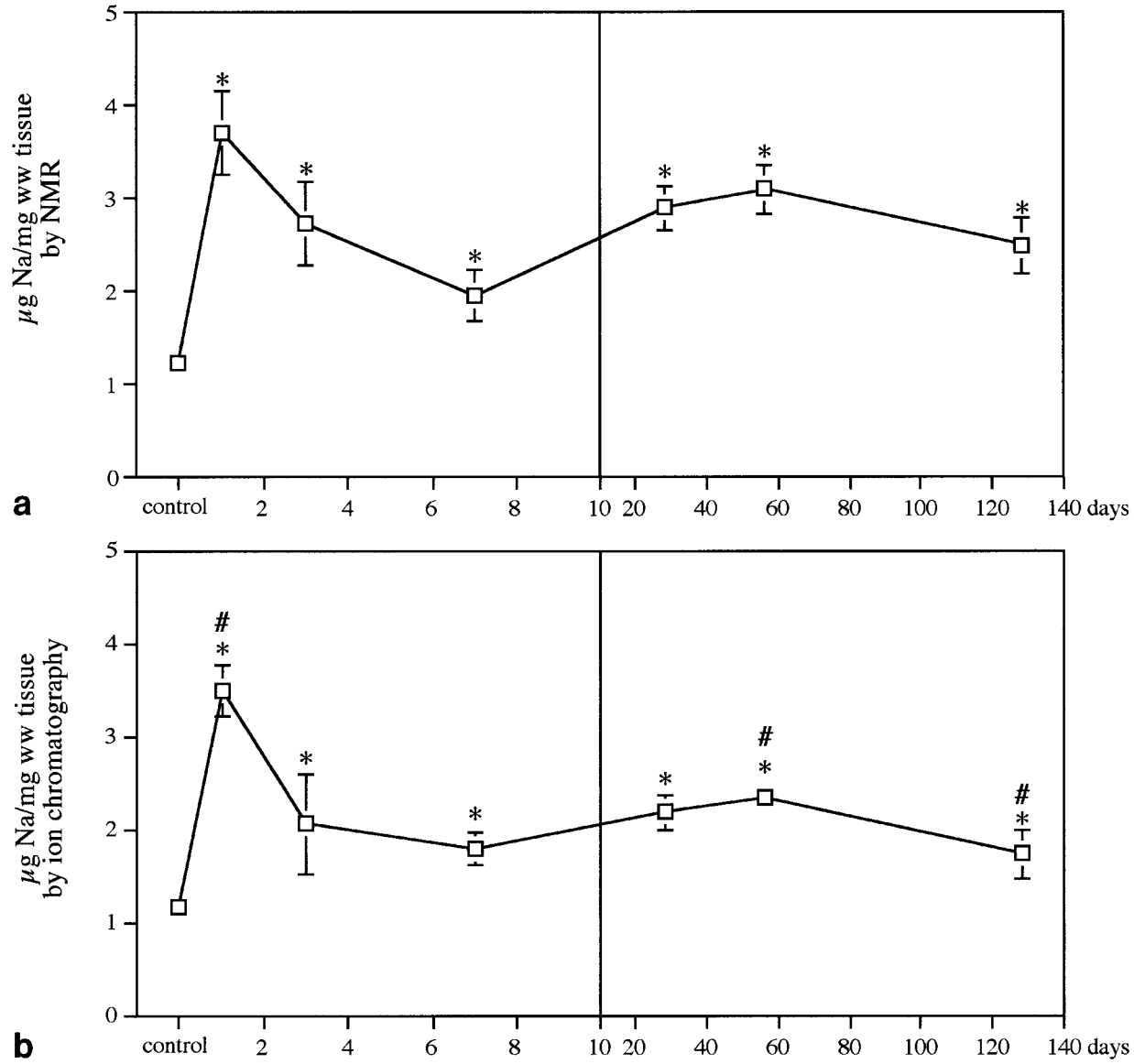


FIG. 1. **a,b:** Total sodium content in control and infarcted myocardium as determined by $^{23}$Na-NMR (upper panel) and ion chromatography (lower panel). The results of $^{23}$Na-MRS and ion chromatography differ 3, 56, and 128 days after myocardial infarction. However, the total Na content is increased in the scar compared to control tissue at all time points. *$P < 0.05$ vs. control, #$P < 0.05$ $^{23}$Na-NMR vs. ion chromatography.

the standard solution at 12 ppm. Mean SNR of the tissue signal was 14.5 ± 1.3.

In control hearts, total sodium content, measured by $^{23}$Na-MRS, averaged 1.16 ± 0.07 μg Na/mg ww tissue. At 1 day post-MI, total sodium in the infarct region was 3.1-fold higher than in the nonischemic control group. Moreover, sodium levels in the infarct/scar were persistently elevated in all MI groups, averaging 230% of control on day 3, and ~170% of control values at days 7, 28, 56, and 128 post-ligation (Fig. 1a).

### *Ion Chromatography*

There was close agreement in the sodium concentrations assessed by ion chromatography (Fig. 1b) vs. sodium content determined by NMR. The temporal profile of Na content was similar using both methods, and all post-MI values were significantly elevated vs. controls. Both methods revealed that, at 1 month after MI, the Na curve reached a plateau and did not change substantially thereafter.

## Protocol 2

### *$^{23}$Na-MRS*

There was no difference in the chemical shift of the resonance in $^{23}$Na-NMR spectra in canine myocardium (Protocol 2) vs. rat heart (Protocol 1). Mean SNR of the tissue signal was 31.4 ± 2.8.

Total $^{23}$Na content of canine myocardium obtained at baseline was 1.042 ± 0.092 μg Na/mg tissue, similar to the Na content observed in control, noninfarcted rat hearts. Na

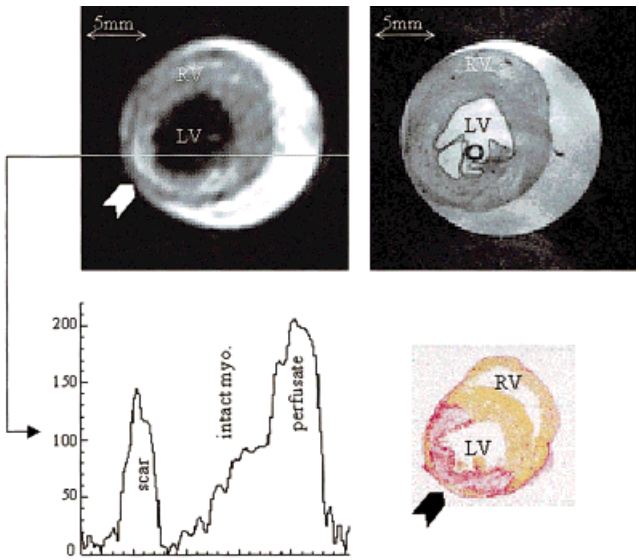


FIG. 2. Top left: $^{23}$Na-MRI (in-plane resolution 0.75 mm * 0.75 mm) in a transversal slice of an isolated rat heart 4 weeks post-MI. The infarct scar appears brighter in the image (marked with arrow); the left ventricular (LV) cavity appears black. Top right: $^{1}$H MRI in the same slice of the heart. The myocardial wall thickness of the infarct scar is slightly reduced. Bottom right: Corresponding Picrosirius Red-stained section. The infarcted area is stained red (marked with arrow). Bottom left: Signal intensity profile in the marked line of the $^{23}$Na image, showing the intensity in the scar, in normal myocardium and in perfusate.

content measured at 3 hours post-stenosis and 30 min after reperfusion (hibernating and stunned myocardium, respectively) averaged 1.015 ± 0.169 and 0.906 ± 0.084 μg Na/mg tissue. That is there was no significant increase in Na concentration in viable but hibernating or in viable but stunned myocardium vs. control.

## Protocol 3

### *Image Quality of $^{23}$Na MRI*

The spatial resolution and SNR of the sodium images allowed clear identification of the LV myocardium, the LV cavity (which appeared black because the balloon inserted for measurement of LV pressures was filled with sodium-free water), and the collapsed right ventricular cavity (Fig. 2).

In each heart, the sodium image was ~40% brighter (i.e., due to signal elevation) in the region of the post-MI scar than in the remaining viable myocardium (Fig. 2). As a result, the scar region was clearly identified. The mean SNR in normal and scarred myocardium and in perfusate, the mean signal intensity (normalized to buffer signal intensity), and the signal elevation and the mean CNR between normal and scarred myocardium are summarized in Table 1.

### *Infarct Size Measurement by $^{23}$Na-MRI*

For each heart, the region exhibiting increased signal intensity in the $^{23}$Na images corresponding to the red-stained (scar) region in the histologic sections (Fig. 3), and to the area with reduced myocardial wall thickness in the proton image. Linear regression analysis revealed a highly significant correlation between infarct size assessed using the two methods ($y = 5.34 + 0.77*x$, $r = 0.91$; $P < 0.0001$; Fig. 4). However, larger infarct sizes were slightly underestimated by $^{23}$Na-MRI.

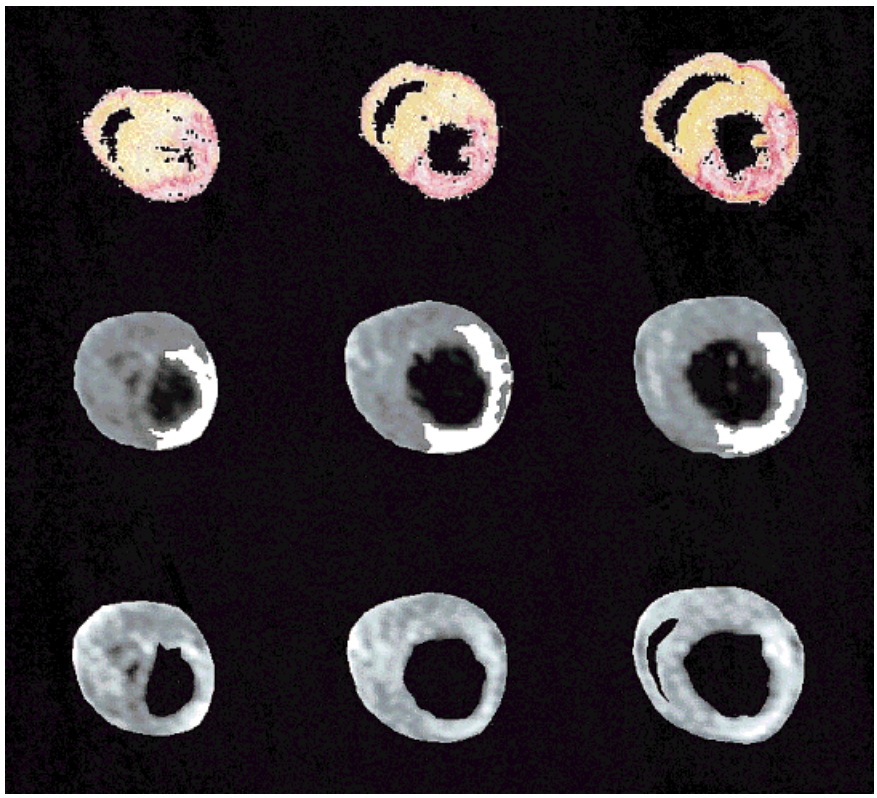

FIG. 3. Left column: three adjacent slices of a 3D $^{23}$Na-MRI dataset in an isolated rat heart 4 weeks post-MI after segmentation. Middle column: The region with signal elevation of double standard deviation over mean in the $^{23}$Na image is delineated in white, and is chosen for infarct size measurement. Right column: corresponding histological slices with stained infarcted area.

Table 1
Summary of Measurements in 15 Slices of $^{23}$Na MRI Dataset in 5 Isolated Rat Hearts 4 Weeks Post MI: Signal-to-Noise Ratio (SNR) in a Region in Normal Myocardium, in Scarred Tissue, in Perfusate and Contrast-to-Noise Ratio (CNR) Between Normal and Scarred Tissue, Signal Intensity in Normal and in Infarcted Tissue Given as % of Buffer Signal Intensity and Resulting Signal Increase

| | Normal | Scar | Perfusate | Normal/scar |
|---|---|---|---|---|
| SNR | 24.1 ± 5.2 | 33.4 ± 4.8 | 53.6 ± 7.9 | — |
| Signal normalized | 50.9 ± 3.4 | 72.2 ± 4.4 | 100 | — |
| CNR | — | — | — | 8.4 ± 3.2 |
| Signal increase % | — | — | — | 42.1 ± 5.7 |

The results are shown as mean ± standard deviation.

## DISCUSSION

In this study, we report that Na content was significant and persistently increased in nonviable (infarcted/scar) vs. viable myocardium. Moreover, at 4 weeks post-MI, $^{23}$Na-MRI yielded an accurate, quantitative assessment of infarct size. There was, however, no difference in Na concentration in viable but stunned or viable but hibernating myocardium vs. control. These data support the concept that $^{23}$Na-MRI may provide a valuable tool for the identification of myocardial infarct/scar tissue and the measurement of infarct size.

### Myocardial Na Content During Post-MI Scar Formation

Our primary aim was to determine whether $^{23}$Na-MRI allows the distinction of nonviable (infarcted/scarred) from viable myocardium with high spatial resolution. Sufficient spatial resolution of $^{23}$Na-MRI can be achieved on whole-body 1.5 T MR systems (16). However, before $^{23}$Na-MRI can be considered as a potential new diagnostic tool, the first issue that must be addressed is whether total myocardial Na content provides sufficient intrinsic contrast for distinguishing scarred tissue from intact tissue.

It is well known that during the initial hours postinfarction, Na content in the necrotic region increases severalfold (20,21). This loss of ion homeostasis is due to inhibition of the Na-K ATPase pump, and additional intracellular influx of Na via the Na-H exchanger (22). In addition to the intracellular increase in Na content, ischemia also leads to extracellular edema, thereby further increasing total tissue Na concentration. Indeed, Kim et al. (7,8) documented an increase in total $^{23}$Na content by MRI during this acute phase of MI.

Although no previous studies have examined the temporal changes in total Na content of infarct/scar tissue beyond the initial days post-MI, the long-term fate of irreversibly damaged myocardium is well described (23,24). After 3 days, neutrophils infiltrate the necrotic tissue, clearing it of dead cardiomyocytes. Simultaneously, fibroblasts migrate to the necrotic zone, producing substantial amounts of collagen and initiating scar formation. Late during the healing process (~6 weeks post-MI), the collagen network stiffens and the number of fibroblasts is reduced, which causes an increase in the extracellular space. In concert, the dry weight/wet weight ratio will be decreased. Our data obtained in Protocol 1 show that, after an initial ~3-fold increase at day 1 post-MI, total Na content plateaued to levels averaging ~170% of control values. This sustained and significant increase in total Na concentration of nonviable vs. viable myocardium provides the necessary, intrinsic contrast required for $^{23}$Na-MRI of the infarct/scar.

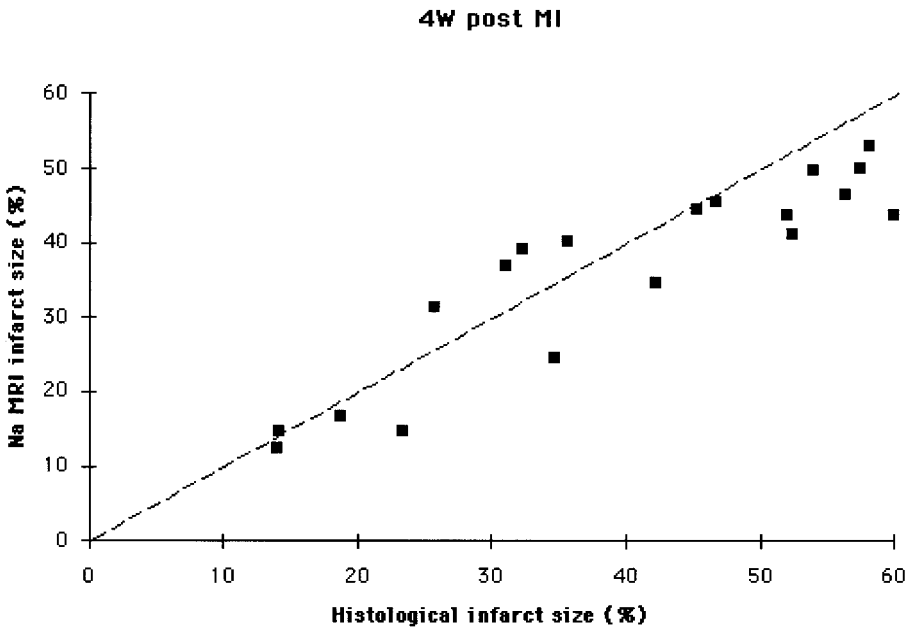


FIG. 4. Size of infarcted area detected with $^{23}$Na-MRI plotted against infarct size determined with histology (Picrosirius Red staining). The dashed line is the line of identity.

We did not specifically determine the reasons for the increased Na content in scar tissue. However, we propose that this may be due to a temporal shift in the volume fraction of intra- vs. extracellular space. Intracellular Na concentrations are in the range of ~10 mM (25), while extracellular Na concentrations are an order of magnitude higher at ~140 mM. In intact myocardium, intra- and extracellular volume each occupy ~50% of total myocardial volume (26). As cardiomyocytes are replaced by fibroblasts and collagen, the extracellular volume fraction increases and intracellular space decreases (22), thereby predicting an increase in total Na content. This was, in fact, confirmed both by $^{23}$Na-MRS and by ion chromatography.

Although the temporal profiles of Na content were virtually identical whether assessed by $^{23}$Na-MRS or ion chromatography, there were modest but significant differences between the two methods at day 3, 2 and 4 months post-MI. Our data cannot explain the difference between absolute values at these three time points. However, we speculate that the increased extracellular volume might be reflected in a larger fraction of slow relaxation (described below), resulting in increased visibility and apparently increased Na content detected by $^{23}$Na-MRS vs. ion chromatography.

## Assessment of Viability by $^{23}$Na-MRI

### *Scar vs. Viable Tissue*

In the present study, using the isolated perfused rat heart model at 11.7 T, image quality achieved by $^{23}$Na-MRI was sufficient to resolve anatomical details. Similar resolution was achieved by Kim et al. (7,8), who reported an increase of Na signal intensity to 142% of control values in the acutely infarcted zone of isolated perfused rabbit hearts.

We found an increase, to 142 ± 6% of control values, in $^{23}$Na image intensity of scar tissue in rat hearts studied 4 weeks post-MI (Protocol 3). Although highly significant, the magnitude of this increase in signal intensity is smaller than the 91% increase in total Na content measured in Protocol 1 with $^{23}$Na-MRS at this same 4-week time point. This apparent discrepancy is, in all likelihood, explained by a methodologic difference between the two protocols: i.e., imaging of excised (nonperfused) scar tissue by MRS vs. imaging of buffer-perfused hearts by MRI. Crystalloid buffer perfusion is well known to cause extracellular edema, resulting in an increase in total Na content in normal myocardium, and thus reducing the contrast between normal and scar tissue (27). Importantly, however, the contrast between normal and scarred myocardium was nonetheless sufficient, even in this buffer-perfused model, to allow for precise delineation of scar tissue based on the criterion of a signal intensity increase larger than 2 standard deviations of the intensity distribution in normal myocardium. Moreover, we obtained a highly significant correlation between histologic and MRI-determined infarct size ($r = 0.91$, $P < 0.0001$), thereby demonstrating the utility of $^{23}$Na-MRI in facilitating a robust and accurate distinction of scar vs. normal myocardium.

### *Stunning/Hibernation*

If myocardial blood flow is compromised due to coronary artery stenosis, the hypoperfused region, although viable, is characterized by depressed mechanical function in concert with reduced metabolic activity (so-called "hibernating" myocardium). Even following full restoration of blood flow, the viable previously ischemic territory remains "stunned" (i.e., exhibits persistent postischemic dysfunction) for hours to days after reperfusion.

In an isolated heart model of reversible ischemia and postischemic stunning, Na content has been shown to rapidly return to normal following reflow (28). Our results, obtained in the canine model (in which stunning and hibernation are well characterized (29)), are consistent with this previous report: under both conditions (stunning and hibernation), total $^{23}$Na content was not increased when compared with control values. That is, $^{23}$Na imaging allows differentiation of infarct/scar tissue from viable myocardium, but does not differentiate viable and intact, viable but hibernating, or viable but stunned regions of the heart. Although clinical confirmation of these observations is required, these results suggest that $^{23}$Na-MRI may provide a useful tool for the assessment of myocardial viability.

## Methodological Aspects

### *$^{23}$Na-MRS*

Due to the quadrupolar nature of $^{23}$Na, there are different types of transitions which might result in fast and slow relaxation of the nuclei. In addition to the narrow spectral lines from slow relaxing transitions, there is signal originating from fast relaxation, causing extremely broad resonances in which accurate integration of the area of the resonance signal is problematic (for a review see Ref. 30). In solutions, 100% of the signal relaxes slowly, while in larger compartments (i.e., the extracellular space) already a certain amount of fast relaxation is reported (31). However, in smaller (intracellular) compartments, reduced mobility of sodium ions might lead to bi-exponential decay of the nuclei, with as much as 60% "invisibility" (20,21,31–42) due to fast relaxation. In our study, however, Na visibility was not a confounding issue: almost all tissue Na was located extracellularly, where visibility is 100%, and invisibility of the small fraction of intracellular Na was quantitatively negligible (approximately 4% of the total Na signal). This is illustrated by the consistency of the results obtained by ion chromatography and $^{23}$Na-MRS.

### *$^{23}$Na-MRI*

Since our MRI experiments were conducted in the isolated buffer-perfused heart model, we believe, as discussed previously, that edema may have partially reduced the contrast between scarred and intact myocardial tissue. In vivo experiments in intact rats would not be affected by this problem, but would require dedicated coil design. A second potential reason for the reduced contrast in the MR images compared to the prediction from MRS analysis is that fast-decaying components of the Na signal cannot be detected with a gradient-echo sequence with a TE of 7 msec. A possible solution is the use of spatially resolved

MRS with a shorter delay between excitation and data acquisition (e.g., 300 μs (17)).

We found that $^{23}$Na-MRI slightly underestimated the size of the largest infarcts. This difference may be explained by the well-documented ~17–24% tissue shrinkage that occurs during formalin fixation and histologic processing (43,44). Inspection of our histologic sections revealed, as expected, an approximate 15% shrinkage in total heart circumference. If there were a difference in shrinkage between scar and intact myocardium, this would contribute to the modest discrepancy in the calculated infarct sizes between the two methods. Nonetheless, our results demonstrate that $^{23}$Na-MRI allows identification of myocardial scar and quantification of infarct size.

## REFERENCES


1. Iskandrian AS, Heo J, Schelbert HR. Myocardial viability: methods of assessment and clinical relevance. Am Heart J 1996;132:1226–1235.
2. Cigarroa CG, deFilippi CR, Brickner ME, Alvarez LG, Wait MA, Grayburn PA. Dobutamine stress echocardiography identifies hibernating myocardium and predicts recovery of left ventricular function after coronary revascularization. Circulation 1993;88:430–436.
3. Akins EW, Hill JA, Sievers KW, Conti CR. Assessment of left ventricular wall thickness in healed myocardial infarction by magnetic resonance imaging. Am J Cardiol 1987;59:24–28.
4. Baer FM, Voth E, Schneider CA, Theissen P, Schicha H, Sechtem U. Comparison of low-dose dobutamine-gradient-echo magnetic resonance imaging and positron emission tomography with [$^{18}$F]fluorodeoxyglucose in patients with chronic coronary artery disease. A functional and morphological approach to the detection of residual myocardial viability. Circulation 1995;91:1006–10015.
5. DeLayre JL, Ingwall JS, Malloy C, Fossel ET. Gated sodium-23 nuclear magnetic resonance images of an isolated perfused working rat heart. Science 1981;212:935–936.
6. Ra JB, Hilal SK, Oh CH, Mun IK. In vivo magnetic resonance imaging of sodium in the human body. Magn Reson Med 1988;7:11–22.
7. Kim R, Lima J, Chen E, Reeder S, Klocke F, Zerhouni E, Judd R. Fast $^{23}$Na magnetic resonance imaging of acute reperfused myocardial infarction. Potential to assess myocardial viability. Circulation 1997;95:1877–1885.
8. Kim R, Judd R, Chen E, Fieno D, Parrish T, JA L. Relationship of elevated $^{23}$Na magnetic resonance image intensity to infarct size after acute reperfused myocardial infarction. Circulation 1999;100:185–192.
9. Cannon PJ, Maudsley AA, Hilal SK, Simon HE, Cassidy F. Sodium nuclear magnetic resonance imaging of myocardial tissue of dogs after coronary artery occlusion and reperfusion. J Am Coll Cardiol 1986;7:573–579.
10. Gaudron P, Hu K, Schamberger R, Budin M, Walter B, Ertl G. Effect of endurance training early or late after coronary artery occlusion on left ventricular remodeling, hemodynamics, and survival in rats with chronic transmural myocardial infarction. Circulation 1994;89:402–412.
11. Pfeffer M, Pfeffer J, Fishbein M, Fletcher P, Spadaro J, Kloner R, Braunwald E. Myocardial infarct size and ventricular function in rats. Circ Res 1979;44:503–512.
12. Horn M, Neubauer S, Frantz S, Hügel S, Hu K, Gaudron P, Schnackerz K, Ertl G. Preservation of left ventricular mechanical function and energy metabolism in rats after myocardial infarction by the angiotensin-converting enzyme inhibitor quinapril. J Cardiovasc Pharmacol 1996;27:201–210.
13. Przyklenk K, Bauer B, Kloner RA. Reperfusion of hibernating myocardium: contractile function, high-energy phosphate content, and myocyte injury after 3 hours of sublethal ischemia and 3 hours of reperfusion in the canine model. Am Heart J 1992;123:575–588.
14. Springer Jr CS, Pike MM, Balschi JA, Chu SC, Frazier JC, Ingwall JS, Smith TW. Use of shift reagents for nuclear magnetic resonance studies of the kinetics of ion transfer in cells and perfused hearts. Circulation 1985;72:Iv89–93.
15. Prince LS, Miller SK, Pohost GM, Elgavish GA. The longitudinal relaxation time (T1) of the intracellular $^{23}$Na NMR signal in the isolated perfused rat heart during hypoxia and reoxygenation. Magn Reson Med 1992;23:376–382.
16. Parrish TB, Fieno DS, Fitzgerald SW, Judd RM. Theoretical basis for sodium and potassium MRI of the human heart at 1.5 T. Magn Reson Med 1997;38:653–661.
17. von Kienlin M, Rösch C, Le Fur Y, Behr W, Roder F, Haase A, Horn M, Illing B, Hu K, Ertl G, Neubauer S. Three-dimensional $^{31}$P magnetic resonance spectroscopic imaging of regional high-energy phosphate metabolism in injured rat heart. Magn Reson Med 1998;39:731–741.
18. Wolff SD, Balaban RS. Magnetization transfer contrast (MTC) and tissue water proton relaxation in vivo. Magn Reson Med 1989;10:135–144.
19. Neubauer S, Horn M, Naumann A, Tian R, Hu K, Laser M, Friedrich J, Gaudron P, Schnackerz K, Ingwall JS, Ertl G. Impairment of energy metabolism in intact residual myocardium of rat hearts with chronic myocardial infarction. J Clin Invest 1995;95:1092–1100.
20. Pike MM, Kitakaze M, Marban E. $^{23}$Na-NMR measurements of intracellular sodium in intact perfused ferret hearts during ischemia and reperfusion. Am J Physiol 1990;259:H1767–H1773.
21. Malloy CR, Buster DC, Castro MM, Geraldes CF, Jeffrey FM, Sherry AD. Influence of global ischemia on intracellular sodium in the perfused rat heart. Magn Reson Med 1990;15:33–44.
22. Opie LH. The heart: physiology, from cell to circulation. Philadelphia: Lippincott Williams & Wilkins; 1997. 637 p.
23. Braunwald E. Heart disease: a textbook of cardiovascular medicine. Philadelphia: W.B. Saunders; 1998.
24. Cleutjens JP, Blankesteijn WM, Daemen MJ, Smits JF. The infarcted myocardium: simply dead tissue, or a lively target for therapeutic interventions? Cardiovasc Res 1999;44:232–241.
25. Ingwall JS. How high does intracellular sodium rise during acute myocardial ischaemia? A view from NMR spectroscopy. Cardiovasc Res 1995;29:279.
26. Nascimben L, Friedrich J, Liao R, Pauletto P, Pessina AC, Ingwall JS. Enalapril treatment increases cardiac performance and energy reserve via the creatine kinase reaction in myocardium of Syrian myopathic hamsters with advanced heart failure. Circulation 1995;91:1824–1833.
27. Döring HJ, Dehnert H. The isolated perfused warm-blooded heart according to Langendorff. Biomesstechnik-Verlag March; 1987. 107 p.
28. Kohler SJ, Perry SB, Stewart LC, Atkinson DE, Clarke K, Ingwall JS. Analysis of $^{23}$Na NMR spectra from isolated perfused hearts. Magn Reson Med 1991;18:15–27.
29. Kloner RA, Bolli R, Marban E, Reinlib L, Braunwald E. Medical and cellular implications of stunning, hibernation, and preconditioning: an NHLBI workshop. Circulation 1998;97:1848–1867.
30. Rooney W, Springer CJ. A comprehensive approach to the analysis and interpretation of the resonances of spins 3/2 from living systems. NMR Biomed 1991;4:209–226.
31. Jelicks LA, Gupta RK. On the extracellular contribution to multiple quantum filtered $^{23}$Na NMR of perfused rat heart. Magn Reson Med 1993;29:130–133.
32. Jelicks LA, Gupta RK. Nuclear magnetic resonance measurement of intracellular sodium in the perfused normotensive and spontaneously hypertensive rat heart. Am J Hypertens 1994;7:429–435.
33. Payne GS, Seymour AM, Styles P, Radda GK. Multiple quantum filtered $^{23}$Na NMR spectroscopy in the perfused heart. NMR Biomed 1990;3:139–146.
34. Schepkin VD, Choy IO, Budinger TF. Sodium alterations in isolated rat heart during cardioplegic arrest. J Appl Physiol 1996;81:2696–2702.
35. Pike MM, Frazer JC, Dedrick DF, Ingwall JS, Allen PD, Springer Jr CS, Smith TW. $^{23}$Na and $^{39}$K nuclear magnetic resonance studies of perfused rat hearts. Discrimination of intra- and extracellular ions using a shift reagent. Biophys J 1985;48:159–173.
36. Jelicks LA, Gupta RK. Multinuclear NMR studies of the Langendorff perfused rat heart. J Biol Chem 1989;264:15230–15235.
37. Pike MM, Luo CS, Yanagida S, Hageman GR, Anderson PG. $^{23}$Na and $^{31}$P nuclear magnetic resonance studies of ischemia-induced ventricular fibrillation. Alterations of intracellular Na+ and cellular energy. Circ Res 1995;77:394–406.

38. Pike MM, Luo CS, Clark MD, Kirk KA, Kitakaze M, Madden MC, Cragoe Jr EJ, Pohost GM. NMR measurements of $Na^+$ and cellular energy in ischemic rat heart: role of $Na^{(+)}$-$H^+$ exchange. Am J Physiol 1993;265: H2017–H2026.
39. Navon G, Werrmann JG, Maron R, Cohen SM. $^{31}P$ NMR and triple quantum filtered $^{23}Na$ NMR studies of the effects of inhibition of $Na^+/H^+$ exchange on intracellular sodium and pH in working and ischemic hearts. Magn Reson Med 1994;32:556–564.
40. Ramasamy R, Liu H, Anderson S, Lundmark J, Schaefer S. Ischemic preconditioning stimulates sodium and proton transport in isolated rat hearts. J Clin Invest 1995;96:1464–1472.
41. van Echteld CJ, Kirkels JH, Eijgelshoven MH, van der Meer P, Ruigrok TJ. Intracellular sodium during ischemia and calcium-free perfusion: a $^{23}Na$ NMR study. J Mol Cell Cardiol 1991;23:297–307.
42. Radford NB, Makos JD, Ramasamy R, Sherry AD, Malloy CR. Dissociation of intracellular sodium from contractile state in guinea-pig hearts treated with ouabain. J Mol Cell Cardiol 1998;30:639–647.
43. McLean M, Prothero J. Three-dimensional reconstruction from serial sections v. calibration of dimensional changes incurred during tissue preparation and data processing. Anal Quant Cytol Histol 1991;13:269–278.
44. Dobrin P. Effect of histological preparation on the cross-sectional area of arterial rings. J Surg Res 1996;61:413–415.